

Universal quantum multi-qubit entangling gates with auxiliary spaces

Wen-Qiang Liu^{1,2}, Hai-Rui Wei^{1,*} and Leong-Chuan Kwek^{3,4,5}

¹*School of Mathematics and Physics, University of Science and Technology Beijing, Beijing 100083, China*

²*Center for Quantum Technology Research and Key Laboratory of Advanced Optoelectronic Quantum Architecture and Measurements (MOE), School of Physics, Beijing Institute of Technology, Beijing 100081, China*

³*Centre for Quantum Technologies, National University of Singapore, Singapore 117543, Singapore*

⁴*MajuLab, CNRS-UNS-NUS-NTU International Joint Research Unit, Singapore UMI 3654, Singapore*

⁵*National Institute of Education and Institute of Advanced Studies, Nanyang Technological University, Singapore 637616, Singapore*

Universal quantum entangling gates are a crucial building block in the large-scale quantum computation and quantum communication, and it is an important task to find simple ways to implement them. Here an effective quantum circuit for the implementation of a controlled-NOT (CNOT) gate is constructed by introducing a non-computational quantum state in the auxiliary space. Furthermore, the method is extended to the construction of a general n -control-qubit Toffoli gate with $(2n - 1)$ qubit-qudit gates and $(2n - 2)$ single-qudit gates. Based on the presented quantum circuits, the polarization CNOT and Toffoli gates with linear optics are designed by operating on the spatial-mode degree of freedom of photons. The proposed optical schemes can be achieved with a higher success probability and no extra auxiliary photons are needed.

Keywords: *quantum computation, quantum circuit, quantum gate, higher-dimensional space, linear optics*

I. INTRODUCTION

Multi-qubit quantum entangling gates have complex structures and play an important role in quantum computing [1], quantum algorithms [2–6], quantum communication [7–16], cryptography [17], etc. [18]. In theory, multi-qubit quantum gates can be realized by sequences of two-qubit gates and single-qubit gates in a quantum circuit model [1]. The cost (also called complexity) of the quantum circuits usually is measured by the number of the two-qubit entangled gates involved in the quantum circuit, because they introduce more imperfections and more demands than the single-qubit gates. However, when the cost of a quantum circuit is high, it is difficult to perform the experiments because of the low computing fidelity and limited coherence time. Moreover, the cost of a universal quantum circuit increases exponentially with the accumulation of the number of qubits. The theoretical lower bound for simulating an n -qubit universal quantum circuit is $(4^n - 3n - 1)/4$ controlled-NOT (CNOT) gates in a qubit system [19]. Hence, it is crucial to find an effective method for building a universal quantum circuit in the simplest possible way.

Several matrix decomposition techniques have been introduced to optimize a large-scale quantum circuit [20–29]. Two-qubit universal quantum circuits have also been constructed with the lowest cost (resources) in qubit systems [19, 30–32]. However, there is still a gap between the current best result [24] and the theoretical lower bound [19] for a multi-qubit universal quantum circuit. Fortunately, Ralph *et al.* [33] found that the quantum circuit may be optimized further by using higher-dimensional Hilbert spaces, and this proposal was later experimentally demonstrated in optical [34] and superconducting systems [35]. Following this, Liu *et al.* [36, 37] reduced the cost of the n -qubit universal circuit to $(5/16) \times 4^n - (5/4) \times 2^n + 2n$ CNOT gates when n was even and $(5/16) \times 4^n - 2^n + 2(n - 1)$ CNOTs when n was odd. Liu *et al.* simplified a Fredkin gate from eight CNOTs to five CNOTs [38] or three qubit-qudit gates [39]. In addition, higher-dimensional quantum systems have also been studied [40, 41] and applied in quantum computing [42–45], quantum communication [46–53], and quantum metrology [54].

The Toffoli (controlled-controlled-NOT) gate, a three-qubit conditional operation, is one of the most popular universal multi-qubit quantum gates [55–57]. It is also an essential component in complex quantum algorithms [2–6], quantum error correction [58, 59], and quantum fault tolerance [60, 61]. In 1995, Barenco *et al.* [1] proposed a concrete construction of a three-qubit Toffoli gate with five two-qubit entangled gates. When two-qubit gates are restricted to CNOT gates, the optimal cost of a Toffoli gate increases to six [62]. In 2013, Yu *et al.* [63, 64] confirmed that the minimum resource for simulating a three-qubit Toffoli gate is five two-qubit gates. In 2020, Kiktenko *et al.* [65] constructed a generalized m -qubit Toffoli gate with $(2m - 3)$ CNOTs based on qudits. Independent of the standard decomposition-based approach, the realization of Toffoli gate has been proposed theoretically and implemented experimentally in superconducting circuits [35, 59], linear optics [34, 42, 66–68], trapped ions [69], atoms [70, 71], and quantum dots [72].

* Corresponding author: hrwei@ustb.edu.cn

Ralph *et al.* [33, 34] first proposed an interesting scheme for synthesizing a Toffoli gate using three qubit-qudit CNOT gates and two single-qudit X_A gates. The main idea of the works in Refs. [33, 34] was to extend temporarily the higher-dimensional subspaces on one of the controlled qubit carriers and then perform corresponding logical operations. Using the same method as Refs. [33, 34], in this paper, we propose an alternative scheme to implement the CNOT and Toffoli gates based on the partial-swap (P-SWAP) gates by using higher-dimensional spaces. Specifically, $(2n-1)$ qubit-qudit and $(2n-2)$ single-qudit gates are required to implement an n -control-qubit Toffoli gate. In addition, using the spatial-mode degree of freedom (DOF) of the single-photon, we design a feasible optical architecture for implementing CNOT and Toffoli gates with linear optics. Our proposals have several other advantages: (i) Our optical implementation of the CNOT gate does not require an extra entangled photon pair or a single-photon, and the success probability of the gate is enhanced. (ii) Linear optical Toffoli gates can be constructed with a higher success probability than other existing optical schemes [33, 34, 73]. (iii) Our schemes are simple and feasible with the current technology.

II. CONSTRUCTION OF CNOT AND TOFFOLI GATES WITH HIGHER-DIMENSIONAL SPACES

A. Synthesis of a CNOT gate using qutrits

A CNOT gate with two P-SWAP gates using qutrits is shown in Figure 1. The gate qubits are encoded on two computational states, $|0\rangle$ and $|1\rangle$. The single-qutrit X_A gate provides a three-dimensional subspace on the control qubit. In the following, we describe the construction process of our protocol in detail.

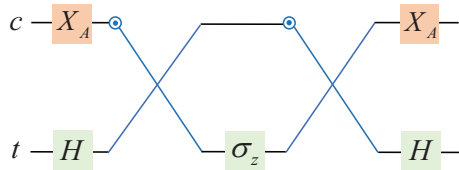


FIG. 1: Synthesis of a CNOT gate. The single-qutrit X_A gate implements the transformation $|1\rangle \leftrightarrow |2\rangle$. The controlled node \odot is turned on for the input $|0\rangle$ or $|1\rangle$. That is, a swap operation is applied to c and t , if and only if, the control qubit c is in the state $|0\rangle$ or $|1\rangle$. H is a single-qubit Hadamard gate to achieve operations $|0\rangle \leftrightarrow \frac{1}{\sqrt{2}}(|0\rangle + |1\rangle)$ and $|1\rangle \leftrightarrow \frac{1}{\sqrt{2}}(|0\rangle - |1\rangle)$. σ_z completes $\sigma_z|0\rangle = |0\rangle$ and $\sigma_z|1\rangle = -|1\rangle$.

Suppose that the state of the system is initially

$$|\phi_0\rangle = \alpha_1|0_c\rangle|0_t\rangle + \alpha_2|0_c\rangle|1_t\rangle + \alpha_3|1_c\rangle|0_t\rangle + \alpha_4|1_c\rangle|1_t\rangle. \quad (1)$$

where α_i ($i = 1, 2, 3, 4$) are complex coefficients that satisfy the normalization condition $\sum_{i=1}^4 |\alpha_i|^2 = 1$. Subscripts c and t denote the control and target qubits, respectively.

First, qubit c undergoes a single-qutrit gate X_A , which introduces an ancillary state $|2\rangle$ on c and completes the transformations $|1_c\rangle \xrightarrow{X_A} |2_c\rangle$ and $|0_c\rangle \xrightarrow{X_A} |0_c\rangle$. After the X_A gate and a Hadamard (H) gate are applied to c and t , the initial state $|\phi_0\rangle$ is changed to

$$|\phi_1\rangle = \frac{1}{\sqrt{2}} [\alpha_1(|0_c\rangle(|0_t\rangle + |1_t\rangle)) + \alpha_2(|0_c\rangle(|0_t\rangle - |1_t\rangle)) + \alpha_3|2_c\rangle(|0_t\rangle + |1_t\rangle) + \alpha_4|2_c\rangle(|0_t\rangle - |1_t\rangle)]. \quad (2)$$

Second, a P-SWAP gate is applied to c and t , and it transforms $|\phi_1\rangle$ into

$$|\phi_2\rangle = \frac{1}{\sqrt{2}} [\alpha_1(|0_c\rangle + |1_c\rangle)|0_t\rangle + \alpha_2(|0_c\rangle - |1_c\rangle)|0_t\rangle + \alpha_3|2_c\rangle(|0_t\rangle + |1_t\rangle) + \alpha_4|2_c\rangle(|0_t\rangle - |1_t\rangle)]. \quad (3)$$

Here, the P-SWAP gate performs a swap operation only between two computational states $|0\rangle$ and $|1\rangle$, that is,

$$\begin{aligned} |00\rangle &\xrightarrow{\text{P-SWAP}} |00\rangle, & |01\rangle &\xrightarrow{\text{P-SWAP}} |10\rangle, \\ |10\rangle &\xrightarrow{\text{P-SWAP}} |01\rangle, & |11\rangle &\xrightarrow{\text{P-SWAP}} |11\rangle, \\ |20\rangle &\xrightarrow{\text{P-SWAP}} |20\rangle, & |21\rangle &\xrightarrow{\text{P-SWAP}} |21\rangle. \end{aligned} \quad (4)$$

Third, a σ_z operation acts on t to change $|\phi_2\rangle$ to

$$|\phi_3\rangle = \frac{1}{\sqrt{2}} [\alpha_1(|0_c\rangle + |1_c\rangle)|0_t\rangle + \alpha_2(|0_c\rangle - |1_c\rangle)|0_t\rangle + \alpha_3|2_c\rangle(|0_t\rangle - |1_t\rangle) + \alpha_4|2_c\rangle(|0_t\rangle + |1_t\rangle)]. \quad (5)$$

Finally, after the P-SWAP gate, the X_A gate and H operation are applied to c and t again, $|\phi_3\rangle$ is changed to

$$|\phi_4\rangle = \alpha_1|0_c\rangle|0_t\rangle + \alpha_2|0_c\rangle|1_t\rangle + \alpha_3|1_c\rangle|1_t\rangle + \alpha_4|1_c\rangle|0_t\rangle. \quad (6)$$

From Equation (1) to Equation (6), one can see that a CNOT gate is completed by Figure 1, and such a construction can be achieved in linear optics with a high success probability and without additional photons (see section III).

B. Construction of the Toffoli gates with higher-dimensional spaces

1. Synthesis of three-qubit Toffoli gate using qutrits

Based on the CNOT and P-SWAP gates, the process for implementing a three-qubit Toffoli gate with four-dimensional space is presented in Figure 2.

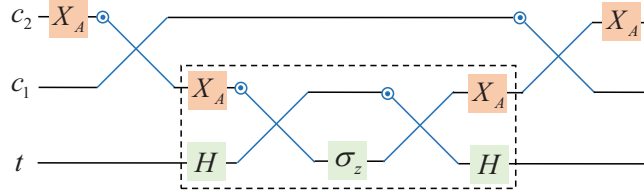


FIG. 2: Simplified synthesis of a three-qubit Toffoli gate with two P-SWAP and one CNOT gates. As shown in Fig. 1, the operations in the dotted rectangle are a CNOT gate.

Considering an arbitrary normalization three-qubit initial state

$$|\psi_0\rangle = \alpha_1|0_{c_1}\rangle|0_{c_2}\rangle|0_t\rangle + \alpha_2|0_{c_1}\rangle|0_{c_2}\rangle|1_t\rangle + \alpha_3|0_{c_1}\rangle|1_{c_2}\rangle|0_t\rangle + \alpha_4|0_{c_1}\rangle|1_{c_2}\rangle|1_t\rangle + \alpha_5|1_{c_1}\rangle|0_{c_2}\rangle|0_t\rangle + \alpha_6|1_{c_1}\rangle|0_{c_2}\rangle|1_t\rangle + \alpha_7|1_{c_1}\rangle|1_{c_2}\rangle|0_t\rangle + \alpha_8|1_{c_1}\rangle|1_{c_2}\rangle|1_t\rangle. \quad (7)$$

First, the X_A gate acts on c_2 to achieve $|1_{c_2}\rangle \xleftrightarrow{X_A} |2_{c_2}\rangle$ and $|0_{c_2}\rangle \xleftrightarrow{X_A} |0_{c_2}\rangle$. After the first P-SWAP gate is executed on c_1 and c_2 , $|\psi_0\rangle$ becomes

$$|\psi_1\rangle = \alpha_1|0_{c_1}\rangle|0_{c_2}\rangle|0_t\rangle + \alpha_2|0_{c_1}\rangle|0_{c_2}\rangle|1_t\rangle + \alpha_3|0_{c_1}\rangle|2_{c_2}\rangle|0_t\rangle + \alpha_4|0_{c_1}\rangle|2_{c_2}\rangle|1_t\rangle + \alpha_5|0_{c_1}\rangle|1_{c_2}\rangle|0_t\rangle + \alpha_6|0_{c_1}\rangle|1_{c_2}\rangle|1_t\rangle + \alpha_7|1_{c_1}\rangle|2_{c_2}\rangle|0_t\rangle + \alpha_8|1_{c_1}\rangle|2_{c_2}\rangle|1_t\rangle. \quad (8)$$

Second, a CNOT gate is applied to c_1 and t (which can be achieved by the circuit in the dotted rectangle), resulting in

$$|\psi_2\rangle = \alpha_1|0_{c_1}\rangle|0_{c_2}\rangle|0_t\rangle + \alpha_2|0_{c_1}\rangle|0_{c_2}\rangle|1_t\rangle + \alpha_3|0_{c_1}\rangle|2_{c_2}\rangle|0_t\rangle + \alpha_4|0_{c_1}\rangle|2_{c_2}\rangle|1_t\rangle + \alpha_5|0_{c_1}\rangle|1_{c_2}\rangle|0_t\rangle + \alpha_6|0_{c_1}\rangle|1_{c_2}\rangle|1_t\rangle + \alpha_7|1_{c_1}\rangle|2_{c_2}\rangle|1_t\rangle + \alpha_8|1_{c_1}\rangle|2_{c_2}\rangle|0_t\rangle. \quad (9)$$

Finally, the P-SWAP and X_A gates are applied again. The two operations induce $|\psi_2\rangle$ as the final state

$$|\psi_3\rangle = \alpha_1|0_{c_1}\rangle|0_{c_2}\rangle|0_t\rangle + \alpha_2|0_{c_1}\rangle|0_{c_2}\rangle|1_t\rangle + \alpha_3|0_{c_1}\rangle|1_{c_2}\rangle|0_t\rangle + \alpha_4|0_{c_1}\rangle|1_{c_2}\rangle|1_t\rangle + \alpha_5|1_{c_1}\rangle|0_{c_2}\rangle|0_t\rangle + \alpha_6|1_{c_1}\rangle|0_{c_2}\rangle|1_t\rangle + \alpha_7|1_{c_1}\rangle|1_{c_2}\rangle|1_t\rangle + \alpha_8|1_{c_1}\rangle|1_{c_2}\rangle|0_t\rangle. \quad (10)$$

From Equations (7-10), one can see that a three-qubit Toffoli gate can be simulated using three nearest-neighbor qubit-qutrit gates and two single-qutrit gates.

2. Synthesis of n -control-qubit Toffoli gate using qudits

Using a higher-dimensional space, the method can be applied to any multi-qubit Toffoli gate. As shown in Figure 3, an n -control-qubit Toffoli gate is constructed with $(2n - 1)$ qubit-qudit and $(2n - 2)$ single-qudit gates, which flips the target qubit states $|0\rangle$ and $|1\rangle$ if and only if the n control-qubits are all $|1\rangle$. Here, single-qudit gates X_a, X_b, \dots, X_n create multi-level qudits on c_n and complete transformations $|0_{c_n}\rangle \leftrightarrow |2_{c_n}\rangle, |1_{c_n}\rangle \leftrightarrow |3_{c_n}\rangle, |0_{c_n}\rangle \leftrightarrow |4_{c_n}\rangle, \dots, |0_{c_n}\rangle \leftrightarrow |n_{c_n}\rangle$ when n is even or $|0_{c_n}\rangle \leftrightarrow |2_{c_n}\rangle, |1_{c_n}\rangle \leftrightarrow |3_{c_n}\rangle, |0_{c_n}\rangle \leftrightarrow |4_{c_n}\rangle, \dots, |1_{c_n}\rangle \leftrightarrow |n_{c_n}\rangle$ when n is odd. These single-qudit gates can temporarily expand the two-dimensional space of c_n to an $(n+1)$ -dimensional subspace. All CNOT and P-SWAP gates act on computational states $|0\rangle$ and $|1\rangle$. The synthesis requires only $O(n)$ qubit-qudit gates and the low-cost advantage is more evident in our scheme as the number of qubits increases.

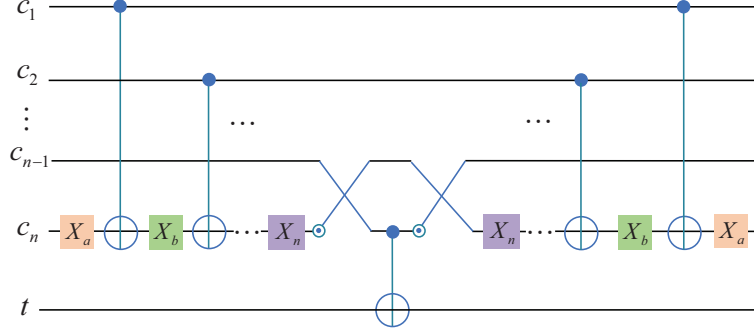


FIG. 3: Synthesis of an n -control-qubit Toffoli gate in a higher-dimensional space. Single-qudit gates X_a, X_b, \dots, X_n complete operations $|0_{c_n}\rangle \leftrightarrow |2_{c_n}\rangle, |1_{c_n}\rangle \leftrightarrow |3_{c_n}\rangle, \dots, |0_{c_n}\rangle \leftrightarrow |n_{c_n}\rangle$ when n is even or $|0_{c_n}\rangle \leftrightarrow |2_{c_n}\rangle, |1_{c_n}\rangle \leftrightarrow |3_{c_n}\rangle, \dots, |1_{c_n}\rangle \leftrightarrow |n_{c_n}\rangle$ when n is odd, respectively.

III. IMPLEMENTATION OF CNOT AND TOFFOLI GATES WITH LINEAR OPTICS

A. Implementation of a post-selected P-SWAP gate with linear optics

In the previous section, we proposed the simulation of CNOT and Toffoli gates based on P-SWAP gates and auxiliary higher-dimensional spaces. In an optical system, two computational states can be encoded on the polarization DOF of a single photon in the spatial-mode i , that is, $|0\rangle \equiv |H\rangle_i$ and $|1\rangle \equiv |V\rangle_i$. Here, H and V represent the horizontal and vertical polarized components, respectively. The higher-dimensional state can be encoded on the V -polarized component in a new spatial-mode i' , that is, $|2\rangle \equiv |V\rangle_{i'}$. The qutrit operation X_A can be achieved by employing a polarizing beam splitter (PBS), which reflects the V -polarized component and transmits the H -polarized component, respectively. Before describing the implementation of the CNOT gate, we first detail the step-by-step construction of the P-SWAP gate with linear optical elements.

As shown in Figure 4, the injected photon 1 is divided into H -polarized component and V -polarized component by a PBS. The H -polarized component passes into the spatial-mode 1_{in} , which is encoded on $|H\rangle_{1_{in}} \equiv |0\rangle$ (and V -polarized component in the spatial-mode 1_{in} is encoded on $|V\rangle_{1_{in}} \equiv |1\rangle$), while the V -polarized component is reflected into another spatial-mode $1'_{in}$, which is encoded on $|V\rangle_{1'_{in}} \equiv |2\rangle$. The photon 2 from the spatial-mode 2_{in} is encoded on $|H\rangle_{2_{in}} \equiv |0\rangle$ and $|V\rangle_{2_{in}} \equiv |1\rangle$. A general injected photon state can be considered as

$$|\varphi_0\rangle = (\alpha_1 \hat{a}_{H1_{in}}^\dagger \hat{a}_{H2_{in}}^\dagger + \alpha_2 \hat{a}_{H1_{in}}^\dagger \hat{a}_{V2_{in}}^\dagger + \alpha_3 \hat{a}_{V1_{in}}^\dagger \hat{a}_{H2_{in}}^\dagger + \alpha_4 \hat{a}_{V1_{in}}^\dagger \hat{a}_{V2_{in}}^\dagger + \alpha_5 \hat{a}_{V1'_{in}}^\dagger \hat{a}_{H2_{in}}^\dagger + \alpha_6 \hat{a}_{V1'_{in}}^\dagger \hat{a}_{V2_{in}}^\dagger) |\text{vac.}\rangle. \quad (11)$$

Here $|\text{vac.}\rangle$ is the state vector of vacuum.

First, PBS₁ and PBS₂ transmit the H -photons into modes 1 and 3 to interact with half-wave plates HWP^{45°} and HWP^{22.5°} and reflect the V -photons into modes 2 and 4 to interact with HWP^{45°} and HWP^{67.5°}. Here, HWP^{45°} is a half-wave plate set to 45 degrees and achieves the qubit-flip operation $\hat{a}_H^\dagger \leftrightarrow \hat{a}_V^\dagger$. HWP^{22.5°} completes the transformations

$$\hat{a}_H^\dagger \xrightarrow{\text{HWP}^{22.5^\circ}} \frac{1}{\sqrt{2}}(\hat{a}_H^\dagger + \hat{a}_V^\dagger), \quad \hat{a}_V^\dagger \xrightarrow{\text{HWP}^{22.5^\circ}} \frac{1}{\sqrt{2}}(\hat{a}_H^\dagger - \hat{a}_V^\dagger). \quad (12)$$

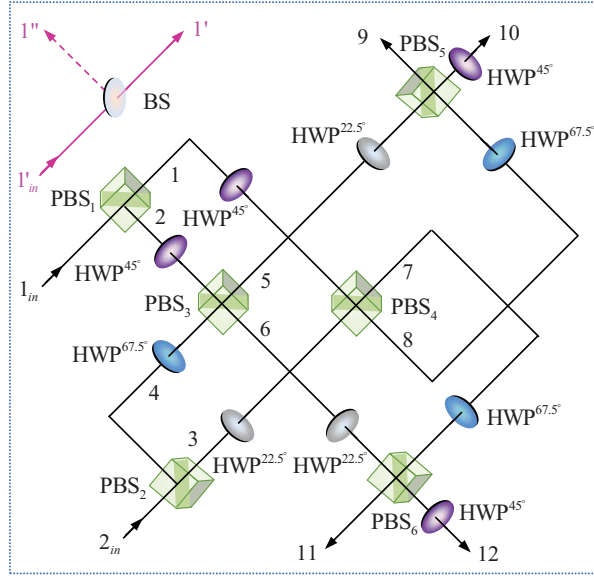


FIG. 4: Implementation of a linear optical P-SWAP gate. The half-wave plate HWP^{45° realizes the qubit-flip $\hat{a}_H^\dagger \leftrightarrow \hat{a}_V^\dagger$. $\text{HWP}^{22.5^\circ}$ completes the operations $\hat{a}_H^\dagger \leftrightarrow \frac{1}{\sqrt{2}}(\hat{a}_H^\dagger + \hat{a}_V^\dagger)$ and $\hat{a}_V^\dagger \leftrightarrow \frac{1}{\sqrt{2}}(\hat{a}_H^\dagger - \hat{a}_V^\dagger)$, and $\text{HWP}^{67.5^\circ}$ completes $\hat{a}_H^\dagger \leftrightarrow \frac{1}{\sqrt{2}}(-\hat{a}_H^\dagger + \hat{a}_V^\dagger)$ and $\hat{a}_V^\dagger \leftrightarrow \frac{1}{\sqrt{2}}(\hat{a}_H^\dagger + \hat{a}_V^\dagger)$. BS is a balanced beam splitter to realize $\hat{a}_{V_1', in}^\dagger \leftrightarrow \frac{1}{\sqrt{2}}(\hat{a}_{V_1'}^\dagger + \hat{a}_{V_1''}^\dagger)$.

$\text{HWP}^{67.5^\circ}$ results in

$$\hat{a}_H^\dagger \xrightarrow{\text{HWP}^{67.5^\circ}} \frac{1}{\sqrt{2}}(-\hat{a}_H^\dagger + \hat{a}_V^\dagger), \quad \hat{a}_V^\dagger \xrightarrow{\text{HWP}^{67.5^\circ}} \frac{1}{\sqrt{2}}(\hat{a}_H^\dagger + \hat{a}_V^\dagger). \quad (13)$$

The above operations, $\text{PBS}_1 \rightarrow \text{HWP}^{45^\circ}$ (HWP^{45°) and $\text{PBS}_2 \rightarrow \text{HWP}^{22.5^\circ}$ ($\text{HWP}^{67.5^\circ}$) cause $|\varphi_0\rangle$ to become

$$\begin{aligned} |\varphi_1\rangle = & \frac{1}{\sqrt{2}} [\alpha_1 \hat{a}_{V_1}^\dagger (\hat{a}_{H_3}^\dagger + \hat{a}_{V_3}^\dagger) + \alpha_2 \hat{a}_{V_1}^\dagger (\hat{a}_{H_4}^\dagger + \hat{a}_{V_4}^\dagger) + \alpha_3 \hat{a}_{H_2}^\dagger (\hat{a}_{H_3}^\dagger + \hat{a}_{V_3}^\dagger) \\ & + \alpha_4 \hat{a}_{H_2}^\dagger (\hat{a}_{H_4}^\dagger + \hat{a}_{V_4}^\dagger) + \alpha_5 \hat{a}_{V_1', in}^\dagger (\hat{a}_{H_3}^\dagger + \hat{a}_{V_3}^\dagger) + \alpha_6 \hat{a}_{V_1', in}^\dagger (\hat{a}_{H_4}^\dagger + \hat{a}_{V_4}^\dagger)] |\text{vac.}\rangle. \end{aligned} \quad (14)$$

Second, photons in mode $1'_{in}$ are then split into modes $1'$ and $1''$ by a balanced polarization beam splitter (BS), i.e., $\hat{a}_{V_1', in}^\dagger \xrightarrow{\text{BS}} (\hat{a}_{V_1'}^\dagger + \hat{a}_{V_1''}^\dagger)/\sqrt{2}$. Photons emitted from modes 2 and 4 (1 and 3) are split into modes 5 and 6 (7 and 8) by PBS_3 (PBS_4) and followed by $\text{HWP}^{22.5^\circ}$ ($\text{HWP}^{67.5^\circ}$). These elements change $|\varphi_1\rangle$ as

$$\begin{aligned} |\varphi_2\rangle = & \frac{1}{2\sqrt{2}} [\alpha_1 (\hat{a}_{H_7}^\dagger + \hat{a}_{V_7}^\dagger) (-\hat{a}_{H_7}^\dagger + \hat{a}_{V_7}^\dagger + \hat{a}_{H_8}^\dagger + \hat{a}_{V_8}^\dagger) + \alpha_2 (\hat{a}_{H_7}^\dagger + \hat{a}_{V_7}^\dagger) (\hat{a}_{H_5}^\dagger + \hat{a}_{V_5}^\dagger + \hat{a}_{H_6}^\dagger - \hat{a}_{V_6}^\dagger) \\ & + \alpha_3 (\hat{a}_{H_6}^\dagger + \hat{a}_{V_6}^\dagger) (-\hat{a}_{H_7}^\dagger + \hat{a}_{V_7}^\dagger + \hat{a}_{H_8}^\dagger + \hat{a}_{V_8}^\dagger) + \alpha_4 (\hat{a}_{H_6}^\dagger + \hat{a}_{V_6}^\dagger) (\hat{a}_{H_5}^\dagger + \hat{a}_{V_5}^\dagger + \hat{a}_{H_6}^\dagger - \hat{a}_{V_6}^\dagger) \\ & + \alpha_5 (\hat{a}_{V_1'}^\dagger + \hat{a}_{V_1''}^\dagger) (-\hat{a}_{H_7}^\dagger + \hat{a}_{V_7}^\dagger + \hat{a}_{H_8}^\dagger + \hat{a}_{V_8}^\dagger) + \alpha_6 (\hat{a}_{V_1'}^\dagger + \hat{a}_{V_1''}^\dagger) (\hat{a}_{H_5}^\dagger + \hat{a}_{V_5}^\dagger + \hat{a}_{H_6}^\dagger - \hat{a}_{V_6}^\dagger)] |\text{vac.}\rangle. \end{aligned} \quad (15)$$

Third, PBS_5 (PBS_6) induces photons into modes 9 and 10 (11 and 12). Photons in modes 10 and 12 will undergo HWP^{45° . Thus, the state of the system evolves as

$$\begin{aligned} |\varphi_3\rangle = & \frac{1}{2\sqrt{2}} [\alpha_1 (\hat{a}_{H_{11}}^\dagger + \hat{a}_{H_{12}}^\dagger) (-\hat{a}_{H_{11}}^\dagger + \hat{a}_{H_{12}}^\dagger + \hat{a}_{H_9}^\dagger + \hat{a}_{H_{10}}^\dagger) + \alpha_2 (\hat{a}_{H_{11}}^\dagger + \hat{a}_{H_{12}}^\dagger) (\hat{a}_{V_{10}}^\dagger + \hat{a}_{V_9}^\dagger + \hat{a}_{V_{12}}^\dagger - \hat{a}_{V_{11}}^\dagger) \\ & + \alpha_3 (\hat{a}_{V_{12}}^\dagger + \hat{a}_{V_{11}}^\dagger) (-\hat{a}_{H_{11}}^\dagger + \hat{a}_{H_{12}}^\dagger + \hat{a}_{H_9}^\dagger + \hat{a}_{H_{10}}^\dagger) + \alpha_4 (\hat{a}_{V_{12}}^\dagger + \hat{a}_{V_{11}}^\dagger) (\hat{a}_{V_{10}}^\dagger + \hat{a}_{V_9}^\dagger + \hat{a}_{V_{12}}^\dagger - \hat{a}_{V_{11}}^\dagger) \\ & + \alpha_5 (\hat{a}_{V_1'}^\dagger + \hat{a}_{V_1''}^\dagger) (-\hat{a}_{H_{11}}^\dagger + \hat{a}_{H_{12}}^\dagger + \hat{a}_{H_9}^\dagger + \hat{a}_{H_{10}}^\dagger) + \alpha_6 (\hat{a}_{V_1'}^\dagger + \hat{a}_{V_1''}^\dagger) (\hat{a}_{V_{10}}^\dagger + \hat{a}_{V_9}^\dagger + \hat{a}_{V_{12}}^\dagger - \hat{a}_{V_{11}}^\dagger)] |\text{vac.}\rangle. \end{aligned} \quad (16)$$

The state $|\varphi_3\rangle$ also has the form

$$\begin{aligned}
|\varphi_3\rangle = & |\varphi_4^1\rangle + |\varphi_4^2\rangle + |\varphi_4^3\rangle + |\varphi_4^4\rangle + \frac{1}{2\sqrt{2}} [\alpha_1(\hat{a}_{H_{11}}^\dagger + \hat{a}_{H_{12}}^\dagger)(-\hat{a}_{H_{11}}^\dagger + \hat{a}_{H_{12}}^\dagger) \\
& + \alpha_2(-\hat{a}_{H_{11}}^\dagger \hat{a}_{V_{11}}^\dagger + \hat{a}_{H_{11}}^\dagger \hat{a}_{V_{12}}^\dagger - \hat{a}_{V_{11}}^\dagger \hat{a}_{H_{12}}^\dagger + \hat{a}_{H_{12}}^\dagger \hat{a}_{V_{12}}^\dagger) \\
& + \alpha_3(-\hat{a}_{H_{11}}^\dagger \hat{a}_{V_{11}}^\dagger + \hat{a}_{V_{11}}^\dagger \hat{a}_{H_{12}}^\dagger - \hat{a}_{H_{11}}^\dagger \hat{a}_{V_{12}}^\dagger + \hat{a}_{H_{12}}^\dagger \hat{a}_{V_{12}}^\dagger) \\
& + \alpha_4(\hat{a}_{V_{12}}^\dagger + \hat{a}_{V_{11}}^\dagger)(\hat{a}_{V_{12}}^\dagger - \hat{a}_{V_{11}}^\dagger) + \alpha_5(\hat{a}_{V_{1'}}^\dagger + \hat{a}_{V_{1''}}^\dagger)(\hat{a}_{H_9}^\dagger + \hat{a}_{H_{10}}^\dagger) \\
& + \alpha_6(\hat{a}_{V_{1'}}^\dagger + \hat{a}_{V_{1''}}^\dagger)(\hat{a}_{V_9}^\dagger + \hat{a}_{V_{10}}^\dagger)] |\text{vac.}\rangle.
\end{aligned} \tag{17}$$

Here the four orthogonal states $|\varphi_4^1\rangle$, $|\varphi_4^2\rangle$, $|\varphi_4^3\rangle$, and $|\varphi_4^4\rangle$ are given by

$$|\varphi_4^1\rangle = \frac{1}{2\sqrt{2}} (\alpha_1 \hat{a}_{H_9}^\dagger \hat{a}_{H_{12}}^\dagger + \alpha_2 \hat{a}_{V_9}^\dagger \hat{a}_{H_{12}}^\dagger + \alpha_3 \hat{a}_{H_9}^\dagger \hat{a}_{V_{12}}^\dagger + \alpha_4 \hat{a}_{V_9}^\dagger \hat{a}_{V_{12}}^\dagger + \alpha_5 \hat{a}_{V_{1'}}^\dagger \hat{a}_{H_{12}}^\dagger + \alpha_6 \hat{a}_{V_{1'}}^\dagger \hat{a}_{V_{12}}^\dagger) |\text{vac.}\rangle, \tag{18}$$

$$|\varphi_4^2\rangle = \frac{1}{2\sqrt{2}} (\alpha_1 \hat{a}_{H_{10}}^\dagger \hat{a}_{H_{12}}^\dagger + \alpha_2 \hat{a}_{V_{10}}^\dagger \hat{a}_{H_{12}}^\dagger + \alpha_3 \hat{a}_{H_{10}}^\dagger \hat{a}_{V_{12}}^\dagger + \alpha_4 \hat{a}_{V_{10}}^\dagger \hat{a}_{V_{12}}^\dagger + \alpha_5 \hat{a}_{V_{1''}}^\dagger \hat{a}_{H_{12}}^\dagger + \alpha_6 \hat{a}_{V_{1''}}^\dagger \hat{a}_{V_{12}}^\dagger) |\text{vac.}\rangle, \tag{19}$$

$$|\varphi_4^3\rangle = \frac{1}{2\sqrt{2}} (\alpha_1 \hat{a}_{H_9}^\dagger \hat{a}_{H_{11}}^\dagger + \alpha_2 \hat{a}_{V_9}^\dagger \hat{a}_{H_{11}}^\dagger + \alpha_3 \hat{a}_{H_9}^\dagger \hat{a}_{V_{11}}^\dagger + \alpha_4 \hat{a}_{V_9}^\dagger \hat{a}_{V_{11}}^\dagger - \alpha_5 \hat{a}_{V_{1'}}^\dagger \hat{a}_{H_{11}}^\dagger - \alpha_6 \hat{a}_{V_{1'}}^\dagger \hat{a}_{V_{11}}^\dagger) |\text{vac.}\rangle, \tag{20}$$

$$|\varphi_4^4\rangle = \frac{1}{2\sqrt{2}} (\alpha_1 \hat{a}_{H_{10}}^\dagger \hat{a}_{H_{11}}^\dagger + \alpha_2 \hat{a}_{V_{10}}^\dagger \hat{a}_{H_{11}}^\dagger + \alpha_3 \hat{a}_{H_{10}}^\dagger \hat{a}_{V_{11}}^\dagger + \alpha_4 \hat{a}_{V_{10}}^\dagger \hat{a}_{V_{11}}^\dagger - \alpha_5 \hat{a}_{V_{1''}}^\dagger \hat{a}_{H_{11}}^\dagger - \alpha_6 \hat{a}_{V_{1''}}^\dagger \hat{a}_{V_{11}}^\dagger) |\text{vac.}\rangle. \tag{21}$$

Based on Equations (18-21), a post-selected P-SWAP gate can be operated correctly in the coincidence basis where the photons act as their own qubits. This means the success of the gate is heralded by a detection of an outing single photon in the desired output ports of the gate (see Table I).

(i) If desired coincidence detections of the output modes are 9, 1', and 12 (outputs 1'', 10, and 11 are discarded), the state $|\varphi_3\rangle$ will collapse into $|\varphi_4^1\rangle$, and the P-SWAP gate is completed.

(ii) If desired coincidence detections of the output modes are 10, 1'', and 12 (outputs 1', 9, and 11 are discarded), the state $|\varphi_3\rangle$ will collapse into $|\varphi_4^2\rangle$, and the P-SWAP gate is completed.

(iii) If desired coincidence detections of the output modes are 9, 1', and 11 (outputs 1'', 10, and 12 are discarded), the state $|\varphi_3\rangle$ will collapse into $|\varphi_4^3\rangle$. And then, a phase flip operation, $\hat{a}_{V_{1'}}^\dagger \xrightarrow{\sigma_z} -\hat{a}_{V_{1'}}^\dagger$, should be applied to complete the P-SWAP gate. Such feed-forward operation σ_z can be easily achieved by setting an HWP^{0°} in output mode 1'. The feed-forward operations can be determined by post-selection principle, moreover, the spatial-mode-based feed-forward operations have been experimentally demonstrated recently [74–77].

(iv) If desired coincidence detections of the output modes are 10, 1'', and 11 (outputs 1', 9, and 12 are discarded), the state $|\varphi_3\rangle$ will collapse into $|\varphi_4^4\rangle$. And then, an HWP^{0°} is set in spatial mode 1'' to complete the P-SWAP gate.

Putting all the pieces together one can find that the quantum circuit shown in Figure 4 completes a linear optical P-SWAP gate in the coincidence basis with a success probability of $4 \times 1/8 = 1/2$. The success (or the output modes) of the scheme can be heralded by using the success instances in the post-selection in the applications.

B. Implementation of a post-selected CNOT gate with linear optics

As shown in Figure 5, a post-selected CNOT gate based on P-SWAP gate can be realized in the coincidence basis with linear optical elements. PBS plays a role in the qutrit X_A to provide an additional spatial mode. The operation in the blue dotted rectangle corresponds to a P-SWAP gate in Figure 4.

TABLE I: Coincident expectation outgoing values for six logic basis inputs.

Input	$\hat{a}_{H_9}^\dagger \hat{a}_{H_{12}}^\dagger$	$a_{V_9}^\dagger a_{H_{12}}^\dagger$	$a_{H_9}^\dagger a_{V_{12}}^\dagger$	$a_{V_9}^\dagger a_{V_{12}}^\dagger$	$a_{V_{1'}}^\dagger a_{H_{12}}^\dagger$	$a_{V_{1''}}^\dagger a_{V_{12}}^\dagger$
	$a_{H_{10}}^\dagger a_{H_{12}}^\dagger$	$a_{V_{10}}^\dagger a_{H_{12}}^\dagger$	$a_{H_{10}}^\dagger a_{V_{12}}^\dagger$	$a_{V_{10}}^\dagger a_{V_{12}}^\dagger$	$a_{V_{1''}}^\dagger a_{H_{12}}^\dagger$	$a_{V_{1'}}^\dagger a_{V_{12}}^\dagger$
	$a_{H_9}^\dagger a_{H_{11}}^\dagger$	$a_{V_9}^\dagger a_{H_{11}}^\dagger$	$a_{H_9}^\dagger a_{V_{11}}^\dagger$	$a_{V_9}^\dagger a_{V_{11}}^\dagger$	$-a_{V_{1'}}^\dagger a_{H_{11}}^\dagger$	$-a_{V_{1''}}^\dagger a_{V_{11}}^\dagger$
	$a_{H_{10}}^\dagger a_{H_{11}}^\dagger$	$a_{V_{10}}^\dagger a_{H_{11}}^\dagger$	$a_{H_{10}}^\dagger a_{V_{11}}^\dagger$	$a_{V_{10}}^\dagger a_{V_{11}}^\dagger$	$-a_{V_{1''}}^\dagger a_{H_{11}}^\dagger$	$-a_{V_{1'}}^\dagger a_{V_{11}}^\dagger$
$a_{H_{1in}}^\dagger a_{H_{2in}}^\dagger$	1/8	0	0	0	0	0
$a_{H_{1in}}^\dagger a_{V_{2in}}^\dagger$	0	1/8	0	0	0	0
$a_{V_{1in}}^\dagger a_{H_{2in}}^\dagger$	0	0	1/8	0	0	0
$a_{V_{1in}}^\dagger a_{V_{2in}}^\dagger$	0	0	0	1/8	0	0
$a_{V_{1'in}}^\dagger a_{H_{2in}}^\dagger$	0	0	0	0	1/8	0
$a_{V_{1'in}}^\dagger a_{V_{2in}}^\dagger$	0	0	0	0	0	1/8

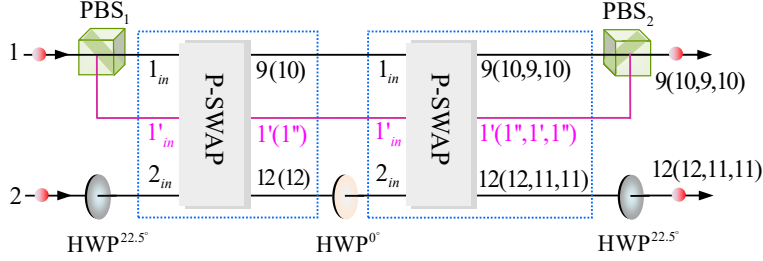


FIG. 5: Implementation of a linear optical CNOT gate. The operation in the dotted rectangle is a P-SWAP gate shown in Fig. 4. Input-output ports pairs mapping $(1_{in}, 1'_{in}, 2_{in}) \rightarrow (9, 1', 12)$ and $(1_{in}, 1'_{in}, 2_{in}) \rightarrow (10, 1'', 12)$ are necessary for the leftmost P-SWAP gate. The outgoing photons from ports $(9, 1', 12)$ and $(10, 1'', 12)$ of the leftmost P-SWAP gate as inputs will route to the next operations. Ports pairs mapping $(1_{in}, 1'_{in}, 2_{in}) \rightarrow (9, 1', 11)$, and $(1_{in}, 1'_{in}, 2_{in}) \rightarrow (10, 1'', 11)$ are employed for the rightmost P-SWAP gate. The outgoing photon pairs emitted from ports pairs $(9, 12)$, $(10, 12)$, $(9, 11)$, and $(10, 11)$ complete the CNOT operation with a success probability of $1/8$.

First, after the two photons are injected into modes 1 and 2, the input state of the system is given by

$$|\chi_0\rangle = (\alpha_1 \hat{a}_{H_1}^\dagger \hat{a}_{H_2}^\dagger + \alpha_2 \hat{a}_{H_1}^\dagger \hat{a}_{V_2}^\dagger + \alpha_3 \hat{a}_{V_1}^\dagger \hat{a}_{H_2}^\dagger + \alpha_4 \hat{a}_{V_1}^\dagger \hat{a}_{V_2}^\dagger) |\text{vac.}\rangle. \quad (22)$$

Second, photons 1 and 2 execute a PBS_1 and an $\text{HWP}^{22.5^\circ}$, respectively, to pass through the leftmost P-SWAP gate. The output ports of the leftmost P-SWAP gate are modes 9, 1', and 12 (or 10, 1'', and 12), which as an input will be led to the next HWP^{0° and the rightmost P-SWAP gate. PBS_1 , $\text{HWP}^{22.5^\circ}$, and the leftmost P-SWAP gate change $|\chi_0\rangle$ into $|\chi_{9,1',12}\rangle$ or $|\chi_{10,1'',12}\rangle$. Here,

$$|\chi_{9,1',12}\rangle_1 = \frac{1}{4} [\alpha_1 (\hat{a}_{H_9}^\dagger + \hat{a}_{V_9}^\dagger) \hat{a}_{H_{12}}^\dagger + \alpha_2 (\hat{a}_{H_9}^\dagger - \hat{a}_{V_9}^\dagger) \hat{a}_{H_{12}}^\dagger + \alpha_3 \hat{a}_{V_{1'}}^\dagger (\hat{a}_{H_{12}}^\dagger + \hat{a}_{V_{12}}^\dagger) + \alpha_4 \hat{a}_{V_{1''}}^\dagger (\hat{a}_{H_{12}}^\dagger - \hat{a}_{V_{12}}^\dagger)] |\text{vac.}\rangle, \quad (23)$$

$$|\chi_{10,1'',12}\rangle_1 = \frac{1}{4} [\alpha_1 (\hat{a}_{H_{10}}^\dagger + \hat{a}_{V_{10}}^\dagger) \hat{a}_{H_{12}}^\dagger + \alpha_2 (\hat{a}_{H_{10}}^\dagger - \hat{a}_{V_{10}}^\dagger) \hat{a}_{H_{12}}^\dagger + \alpha_3 \hat{a}_{V_{1''}}^\dagger (\hat{a}_{H_{12}}^\dagger + \hat{a}_{V_{12}}^\dagger) + \alpha_4 \hat{a}_{V_{1'}}^\dagger (\hat{a}_{H_{12}}^\dagger - \hat{a}_{V_{12}}^\dagger)] |\text{vac.}\rangle. \quad (24)$$

Third, HWP^{0° acts on mode 12 to complete $\hat{a}_{H_{12}}^\dagger \rightarrow \hat{a}_{H_{12}}^\dagger$ and $\hat{a}_{V_{12}}^\dagger \rightarrow -\hat{a}_{V_{12}}^\dagger$. The second P-SWAP gate produces eight desired outcomes of the system, that is, (i) if the desired coincidence detections of the output modes in the second P-SWAP gate are 9, 1', and 12, the state $|\chi_{9,1',12}\rangle_1$ and $|\chi_{10,1'',12}\rangle_1$ both become

$$|\chi_{9,1',12}\rangle_2 = \frac{1}{8\sqrt{2}} [\alpha_1 \hat{a}_{H_9}^\dagger (\hat{a}_{H_{12}}^\dagger + \hat{a}_{V_{12}}^\dagger) + \alpha_2 \hat{a}_{H_9}^\dagger (\hat{a}_{H_{12}}^\dagger - \hat{a}_{V_{12}}^\dagger) + \alpha_3 \hat{a}_{V_{1'}}^\dagger (\hat{a}_{H_{12}}^\dagger - \hat{a}_{V_{12}}^\dagger) + \alpha_4 \hat{a}_{V_{1''}}^\dagger (\hat{a}_{H_{12}}^\dagger + \hat{a}_{V_{12}}^\dagger)] |\text{vac.}\rangle. \quad (25)$$

(ii) If the desired coincidence detections of the output modes in the second P-SWAP gate are 10, 1'', and 12, the state $|\chi_{9,1',12}\rangle_1$ and $|\chi_{10,1'',12}\rangle_1$ both become

$$|\chi_{10,1'',12}\rangle_2 = \frac{1}{8\sqrt{2}} [\alpha_1 \hat{a}_{H_{10}}^\dagger (\hat{a}_{H_{12}}^\dagger + \hat{a}_{V_{12}}^\dagger) + \alpha_2 \hat{a}_{H_{10}}^\dagger (\hat{a}_{H_{12}}^\dagger - \hat{a}_{V_{12}}^\dagger) + \alpha_3 \hat{a}_{V_{1''}}^\dagger (\hat{a}_{H_{12}}^\dagger - \hat{a}_{V_{12}}^\dagger) + \alpha_4 \hat{a}_{V_{1''}}^\dagger (\hat{a}_{H_{12}}^\dagger + \hat{a}_{V_{12}}^\dagger)] |\text{vac.}\rangle. \quad (26)$$

(iii) If the desired coincidence detections of the output modes in the second P-SWAP gate are 9, 1'', and 11, the state $|\chi_{9,1',12}\rangle_1$ and $|\chi_{10,1'',12}\rangle_1$ both become

$$|\chi_{9,1',11}\rangle_2 = \frac{1}{8\sqrt{2}} [\alpha_1 \hat{a}_{H_9}^\dagger (\hat{a}_{H_{11}}^\dagger + \hat{a}_{V_{11}}^\dagger) + \alpha_2 \hat{a}_{H_9}^\dagger (\hat{a}_{H_{11}}^\dagger - \hat{a}_{V_{11}}^\dagger) - \alpha_3 \hat{a}_{V_{1''}}^\dagger (\hat{a}_{H_{11}}^\dagger - \hat{a}_{V_{11}}^\dagger) - \alpha_4 \hat{a}_{V_{1''}}^\dagger (\hat{a}_{H_{11}}^\dagger + \hat{a}_{V_{11}}^\dagger)] |\text{vac.}\rangle. \quad (27)$$

(iv) If the desired coincidence detections of the output modes in the second P-SWAP gate are 10, 1'', and 11, the state $|\chi_{9,1',12}\rangle_1$ and $|\chi_{10,1'',12}\rangle_1$ both become

$$|\chi_{10,1'',11}\rangle_2 = \frac{1}{8\sqrt{2}} [\alpha_1 \hat{a}_{H_{10}}^\dagger (\hat{a}_{H_{11}}^\dagger + \hat{a}_{V_{11}}^\dagger) + \alpha_2 \hat{a}_{H_{10}}^\dagger (\hat{a}_{H_{11}}^\dagger - \hat{a}_{V_{11}}^\dagger) - \alpha_3 \hat{a}_{V_{1''}}^\dagger (\hat{a}_{H_{11}}^\dagger - \hat{a}_{V_{11}}^\dagger) - \alpha_4 \hat{a}_{V_{1''}}^\dagger (\hat{a}_{H_{11}}^\dagger + \hat{a}_{V_{11}}^\dagger)] |\text{vac.}\rangle. \quad (28)$$

Fourth, as shown in Figure 5, PBS₂ leads the photons in modes 9 (i.e., $\hat{a}_{H_9}^\dagger |\text{vac.}\rangle$) and 1' (i.e., $\hat{a}_{V_{1'}}^\dagger |\text{vac.}\rangle$) into one output mode, and combines the photons in modes 10 (i.e., $\hat{a}_{H_{10}}^\dagger |\text{vac.}\rangle$) and 1'' (i.e., $\hat{a}_{V_{1''}}^\dagger |\text{vac.}\rangle$) into one output mode. After PBS₂ and HWP^{22.5°}, (i) Equation (25) evolves into two-fold output state

$$|\chi_{9,12}\rangle_3 = \frac{1}{8} (\alpha_1 \hat{a}_{H_9}^\dagger \hat{a}_{H_{12}}^\dagger + \alpha_2 \hat{a}_{H_9}^\dagger \hat{a}_{V_{12}}^\dagger + \alpha_3 \hat{a}_{V_9}^\dagger \hat{a}_{V_{12}}^\dagger + \alpha_4 \hat{a}_{V_9}^\dagger \hat{a}_{H_{12}}^\dagger) |\text{vac.}\rangle. \quad (29)$$

The CNOT gate is completed. (ii) Equation (26) evolves into two-fold output state

$$|\chi_{10,12}\rangle_3 = \frac{1}{8} (\alpha_1 \hat{a}_{H_{10}}^\dagger \hat{a}_{H_{12}}^\dagger + \alpha_2 \hat{a}_{H_{10}}^\dagger \hat{a}_{V_{12}}^\dagger + \alpha_3 \hat{a}_{V_{10}}^\dagger \hat{a}_{V_{12}}^\dagger + \alpha_4 \hat{a}_{V_{10}}^\dagger \hat{a}_{H_{12}}^\dagger) |\text{vac.}\rangle. \quad (30)$$

The CNOT gate is completed. (iii) Equation (27) evolves into two-fold output state

$$|\chi_{9,11}\rangle_3 = \frac{1}{8} (\alpha_1 \hat{a}_{H_9}^\dagger \hat{a}_{H_{11}}^\dagger + \alpha_2 \hat{a}_{H_9}^\dagger \hat{a}_{V_{11}}^\dagger - \alpha_3 \hat{a}_{V_9}^\dagger \hat{a}_{V_{11}}^\dagger - \alpha_4 \hat{a}_{V_9}^\dagger \hat{a}_{H_{11}}^\dagger) |\text{vac.}\rangle. \quad (31)$$

And then an HWP^{0°} is set in the output mode 9 to complete the CNOT gate. (iv) Equation (28) evolves into two-fold output state

$$|\chi_{10,11}\rangle_3 = \frac{1}{8} (\alpha_1 \hat{a}_{H_{10}}^\dagger \hat{a}_{H_{11}}^\dagger + \alpha_2 \hat{a}_{H_{10}}^\dagger \hat{a}_{V_{11}}^\dagger - \alpha_3 \hat{a}_{V_{10}}^\dagger \hat{a}_{V_{11}}^\dagger - \alpha_4 \hat{a}_{V_{10}}^\dagger \hat{a}_{H_{11}}^\dagger) |\text{vac.}\rangle. \quad (32)$$

And then an HWP^{0°} is set in the output mode 10 to complete the CNOT gate.

Based on above orthogonal two-fold states $|\chi_{9,12}\rangle_3$, $|\chi_{10,12}\rangle_3$, $|\chi_{9,11}\rangle_3$, and $|\chi_{10,11}\rangle_3$, one can find that after the feed-forward operations are only applied to the rightmost P-SWAP gate, an optical post-selected CNOT gate can be operated correctly with a success probability of $8 \times 1/64 = 1/8$. Remarkably, additional entangled photon pairs or single photons are necessary for previous schemes [74–79], but are not required for our CNOT gate. In addition, the success probability of the gate is improved on the results without an auxiliary photon [80–84]. We also note that other method for implementing linear optical CNOT gate with additional DOFs has been demonstrated experimentally [85].

C. Implementation of a post-selected Toffoli gate with linear optics

We propose the implementation of a Toffoli gate based on the designed P-SWAP and CNOT gates. As shown in Figure 6, three photons are injected into modes 1, 2, and 3, simultaneously, the initial state is given by

$$|\Xi_0\rangle = (\alpha_1 \hat{a}_{H_1}^\dagger \hat{a}_{H_2}^\dagger \hat{a}_{H_3}^\dagger + \alpha_2 \hat{a}_{H_1}^\dagger \hat{a}_{H_2}^\dagger \hat{a}_{V_3}^\dagger + \alpha_3 \hat{a}_{H_1}^\dagger \hat{a}_{V_2}^\dagger \hat{a}_{H_3}^\dagger + \alpha_4 \hat{a}_{H_1}^\dagger \hat{a}_{V_2}^\dagger \hat{a}_{V_3}^\dagger + \alpha_5 \hat{a}_{V_1}^\dagger \hat{a}_{H_2}^\dagger \hat{a}_{H_3}^\dagger + \alpha_6 \hat{a}_{V_1}^\dagger \hat{a}_{H_2}^\dagger \hat{a}_{V_3}^\dagger + \alpha_7 \hat{a}_{V_1}^\dagger \hat{a}_{V_2}^\dagger \hat{a}_{H_3}^\dagger + \alpha_8 \hat{a}_{V_1}^\dagger \hat{a}_{V_2}^\dagger \hat{a}_{V_3}^\dagger) |\text{vac.}\rangle. \quad (33)$$

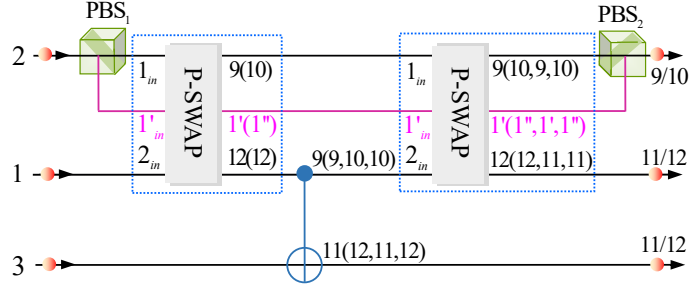


FIG. 6: Optical implementation of a three-photon Toffoli gate.

First, after photons go through the PBS₁ and the leftmost P-SWAP gate, if the output modes of the leftmost P-SWAP gate are 9, 1', and 12, (10, 1'', and 12) and we can obtain two desired states,

$$|\Xi_{1a}\rangle = \frac{1}{2\sqrt{2}} (\alpha_1 \hat{a}_{H_{12}}^\dagger \hat{a}_{H_9}^\dagger \hat{a}_{H_3}^\dagger + \alpha_2 \hat{a}_{H_{12}}^\dagger \hat{a}_{H_9}^\dagger \hat{a}_{V_3}^\dagger + \alpha_3 \hat{a}_{H_{12}}^\dagger \hat{a}_{V_1}^\dagger \hat{a}_{H_3}^\dagger + \alpha_4 \hat{a}_{H_{12}}^\dagger \hat{a}_{V_1}^\dagger \hat{a}_{V_3}^\dagger + \alpha_5 \hat{a}_{H_{12}}^\dagger \hat{a}_{V_9}^\dagger \hat{a}_{H_3}^\dagger + \alpha_6 \hat{a}_{H_{12}}^\dagger \hat{a}_{V_9}^\dagger \hat{a}_{V_3}^\dagger + \alpha_7 \hat{a}_{V_{12}}^\dagger \hat{a}_{V_1}^\dagger \hat{a}_{H_3}^\dagger + \alpha_8 \hat{a}_{V_{12}}^\dagger \hat{a}_{V_1}^\dagger \hat{a}_{V_3}^\dagger) |\text{vac.}\rangle, \quad (34)$$

$$|\Xi_{1b}\rangle = \frac{1}{2\sqrt{2}} (\alpha_1 \hat{a}_{H_{12}}^\dagger \hat{a}_{H_{10}}^\dagger \hat{a}_{H_3}^\dagger + \alpha_2 \hat{a}_{H_{12}}^\dagger \hat{a}_{H_{10}}^\dagger \hat{a}_{V_3}^\dagger + \alpha_3 \hat{a}_{H_{12}}^\dagger \hat{a}_{V_{1'}}^\dagger \hat{a}_{H_3}^\dagger + \alpha_4 \hat{a}_{H_{12}}^\dagger \hat{a}_{V_{1'}}^\dagger \hat{a}_{V_3}^\dagger + \alpha_5 \hat{a}_{H_{12}}^\dagger \hat{a}_{V_{10}}^\dagger \hat{a}_{H_3}^\dagger + \alpha_6 \hat{a}_{H_{12}}^\dagger \hat{a}_{V_{10}}^\dagger \hat{a}_{V_3}^\dagger + \alpha_7 \hat{a}_{V_{12}}^\dagger \hat{a}_{V_{1''}}^\dagger \hat{a}_{H_3}^\dagger + \alpha_8 \hat{a}_{V_{12}}^\dagger \hat{a}_{V_{1''}}^\dagger \hat{a}_{V_3}^\dagger) |\text{vac.}\rangle. \quad (35)$$

Second, the states described by Equation (34) and Equation (35) are employed as the initial states for the next CNOT gate acting on photon 1 and photon 3. If the outgoing photons emitted from path pairs (9, 11), or (9, 12), or (10, 11), or (10, 12), which can yield 16 desired states $|\Xi_{i,9,k}\rangle_1$ (two-fold) and $|\Xi_{i,10,k}\rangle_1$ (two-fold). Here, $|\Xi_{i,9,k}\rangle_1$ and $|\Xi_{i,10,k}\rangle_1$ with $i \in \{9, 10\}$ and $k \in \{11, 12\}$ are described by

$$|\Xi_{i,9,k}\rangle_1 = \frac{1}{16\sqrt{2}} (\alpha_1 \hat{a}_{H_i}^\dagger \hat{a}_{H_9}^\dagger \hat{a}_{H_k}^\dagger + \alpha_2 \hat{a}_{H_i}^\dagger \hat{a}_{H_9}^\dagger \hat{a}_{V_k}^\dagger + \alpha_3 \hat{a}_{H_i}^\dagger \hat{a}_{V_{1'}}^\dagger \hat{a}_{H_k}^\dagger + \alpha_4 \hat{a}_{H_i}^\dagger \hat{a}_{V_{1'}}^\dagger \hat{a}_{V_k}^\dagger + \alpha_5 \hat{a}_{H_i}^\dagger \hat{a}_{V_9}^\dagger \hat{a}_{H_k}^\dagger + \alpha_6 \hat{a}_{H_i}^\dagger \hat{a}_{V_9}^\dagger \hat{a}_{V_k}^\dagger + \alpha_7 \hat{a}_{V_i}^\dagger \hat{a}_{V_{1'}}^\dagger \hat{a}_{V_k}^\dagger + \alpha_8 \hat{a}_{V_i}^\dagger \hat{a}_{V_{1'}}^\dagger \hat{a}_{H_k}^\dagger) |\text{vac.}\rangle, \quad (36)$$

$$|\Xi_{i,10,k}\rangle_1 = \frac{1}{16\sqrt{2}} (\alpha_1 \hat{a}_{H_i}^\dagger \hat{a}_{H_{10}}^\dagger \hat{a}_{H_k}^\dagger + \alpha_2 \hat{a}_{H_i}^\dagger \hat{a}_{H_{10}}^\dagger \hat{a}_{V_k}^\dagger + \alpha_3 \hat{a}_{H_i}^\dagger \hat{a}_{V_{1''}}^\dagger \hat{a}_{H_k}^\dagger + \alpha_4 \hat{a}_{H_i}^\dagger \hat{a}_{V_{1''}}^\dagger \hat{a}_{V_k}^\dagger + \alpha_5 \hat{a}_{H_i}^\dagger \hat{a}_{V_{10}}^\dagger \hat{a}_{H_k}^\dagger + \alpha_6 \hat{a}_{H_i}^\dagger \hat{a}_{V_{10}}^\dagger \hat{a}_{V_k}^\dagger + \alpha_7 \hat{a}_{V_i}^\dagger \hat{a}_{V_{1''}}^\dagger \hat{a}_{V_k}^\dagger + \alpha_8 \hat{a}_{V_i}^\dagger \hat{a}_{V_{1''}}^\dagger \hat{a}_{H_k}^\dagger) |\text{vac.}\rangle. \quad (37)$$

Third, above 16 states are introduced as the initial states for the rightmost P-SWAP gate acting on photon 1 and photon 2. If coincidence detection mode pairs are (9, 1', and 12), or (9, 1', and 11), or (10, 1'', and 12), or (10, 1'', and 11), we can obtain 64 desired states $|\Xi_{12,9,k}^+\rangle_2$, $|\Xi_{12,10,k}^+\rangle_2$, $|\Xi_{11,9,k}^-\rangle_2$ and $|\Xi_{11,10,k}^-\rangle_2$. Here, eight-fold states $|\Xi_{12,9,k}^+\rangle_2$, $|\Xi_{12,10,k}^+\rangle_2$, $|\Xi_{11,9,k}^-\rangle_2$, and $|\Xi_{11,10,k}^-\rangle_2$ with $k \in \{11, 12\}$ are described by

$$|\Xi_{12,9,k}^+\rangle_2 = \frac{1}{64} (\alpha_1 \hat{a}_{H_{12}}^\dagger \hat{a}_{H_9}^\dagger \hat{a}_{H_k}^\dagger + \alpha_2 \hat{a}_{H_{12}}^\dagger \hat{a}_{H_9}^\dagger \hat{a}_{V_k}^\dagger + \alpha_3 \hat{a}_{H_{12}}^\dagger \hat{a}_{V_{1'}}^\dagger \hat{a}_{H_k}^\dagger + \alpha_4 \hat{a}_{H_{12}}^\dagger \hat{a}_{V_{1'}}^\dagger \hat{a}_{V_k}^\dagger + \alpha_5 \hat{a}_{V_{12}}^\dagger \hat{a}_{H_9}^\dagger \hat{a}_{H_k}^\dagger + \alpha_6 \hat{a}_{V_{12}}^\dagger \hat{a}_{H_9}^\dagger \hat{a}_{V_k}^\dagger + \alpha_7 \hat{a}_{V_{12}}^\dagger \hat{a}_{V_{1'}}^\dagger \hat{a}_{V_k}^\dagger + \alpha_8 \hat{a}_{V_{12}}^\dagger \hat{a}_{V_{1'}}^\dagger \hat{a}_{H_k}^\dagger) |\text{vac.}\rangle, \quad (38)$$

$$|\Xi_{12,10,k}^+\rangle_2 = \frac{1}{64} (\alpha_1 \hat{a}_{H_{12}}^\dagger \hat{a}_{H_{10}}^\dagger \hat{a}_{H_k}^\dagger + \alpha_2 \hat{a}_{H_{12}}^\dagger \hat{a}_{H_{10}}^\dagger \hat{a}_{V_k}^\dagger + \alpha_3 \hat{a}_{H_{12}}^\dagger \hat{a}_{V_{1''}}^\dagger \hat{a}_{H_k}^\dagger + \alpha_4 \hat{a}_{H_{12}}^\dagger \hat{a}_{V_{1''}}^\dagger \hat{a}_{V_k}^\dagger + \alpha_5 \hat{a}_{V_{12}}^\dagger \hat{a}_{H_{10}}^\dagger \hat{a}_{H_k}^\dagger + \alpha_6 \hat{a}_{V_{12}}^\dagger \hat{a}_{H_{10}}^\dagger \hat{a}_{V_k}^\dagger + \alpha_7 \hat{a}_{V_{12}}^\dagger \hat{a}_{V_{1''}}^\dagger \hat{a}_{V_k}^\dagger + \alpha_8 \hat{a}_{V_{12}}^\dagger \hat{a}_{V_{1''}}^\dagger \hat{a}_{H_k}^\dagger) |\text{vac.}\rangle, \quad (39)$$

$$|\Xi_{11,9,k}^-\rangle_2 = \frac{1}{64} (\alpha_1 \hat{a}_{H_{11}}^\dagger \hat{a}_{H_9}^\dagger \hat{a}_{H_k}^\dagger + \alpha_2 \hat{a}_{H_{11}}^\dagger \hat{a}_{H_9}^\dagger \hat{a}_{V_k}^\dagger - \alpha_3 \hat{a}_{H_{11}}^\dagger \hat{a}_{V_{1'}}^\dagger \hat{a}_{H_k}^\dagger - \alpha_4 \hat{a}_{H_{11}}^\dagger \hat{a}_{V_{1'}}^\dagger \hat{a}_{V_k}^\dagger + \alpha_5 \hat{a}_{V_{11}}^\dagger \hat{a}_{H_9}^\dagger \hat{a}_{H_k}^\dagger + \alpha_6 \hat{a}_{V_{11}}^\dagger \hat{a}_{H_9}^\dagger \hat{a}_{V_k}^\dagger - \alpha_7 \hat{a}_{V_{11}}^\dagger \hat{a}_{V_{1'}}^\dagger \hat{a}_{H_k}^\dagger - \alpha_8 \hat{a}_{V_{11}}^\dagger \hat{a}_{V_{1'}}^\dagger \hat{a}_{V_k}^\dagger) |\text{vac.}\rangle, \quad (40)$$

$$\begin{aligned}
|\Xi_{11,10,k}^-\rangle_2 = \frac{1}{64} & (\alpha_1 \hat{a}_{H_{11}}^\dagger \hat{a}_{H_{10}}^\dagger \hat{a}_{H_k}^\dagger + \alpha_2 \hat{a}_{H_{11}}^\dagger \hat{a}_{H_{10}}^\dagger \hat{a}_{V_k}^\dagger - \alpha_3 \hat{a}_{H_{11}}^\dagger \hat{a}_{V_{1''}}^\dagger \hat{a}_{H_k}^\dagger - \alpha_4 \hat{a}_{H_{11}}^\dagger \hat{a}_{V_{1''}}^\dagger \hat{a}_{V_k}^\dagger \\
& + \alpha_5 \hat{a}_{V_{11}}^\dagger \hat{a}_{H_{10}}^\dagger \hat{a}_{H_k}^\dagger + \alpha_6 \hat{a}_{V_{11}}^\dagger \hat{a}_{H_{10}}^\dagger \hat{a}_{V_k}^\dagger - \alpha_7 \hat{a}_{V_{11}}^\dagger \hat{a}_{V_{1''}}^\dagger \hat{a}_{V_k}^\dagger - \alpha_8 \hat{a}_{V_{11}}^\dagger \hat{a}_{V_{1''}}^\dagger \hat{a}_{H_k}^\dagger) |\text{vac.}\rangle.
\end{aligned} \tag{41}$$

Finally, as shown in Figure 6, the photons emitted from modes 9 (i.e., $\hat{a}_{H_9}^\dagger |\text{vac.}\rangle$) and 1' (i.e., $\hat{a}_{V_{1'}}^\dagger |\text{vac.}\rangle$) are combined into the same output mode by PBS₂. The photons emitted from modes 10 (i.e., $\hat{a}_{H_{10}}^\dagger |\text{vac.}\rangle$) and 1'' ($\hat{a}_{V_{1''}}^\dagger |\text{vac.}\rangle$) are also led to the same output mode by PBS₂. Therefore, after PBS₂, (i) Equation (38) evolves into eight-fold output state

$$\begin{aligned}
|\Xi_{12,9,k}^+\rangle_3 = \frac{1}{64} & (\alpha_1 \hat{a}_{H_{12}}^\dagger \hat{a}_{H_9}^\dagger \hat{a}_{H_k}^\dagger + \alpha_2 \hat{a}_{H_{12}}^\dagger \hat{a}_{H_9}^\dagger \hat{a}_{V_k}^\dagger + \alpha_3 \hat{a}_{H_{12}}^\dagger \hat{a}_{V_9}^\dagger \hat{a}_{H_k}^\dagger + \alpha_4 \hat{a}_{H_{12}}^\dagger \hat{a}_{V_9}^\dagger \hat{a}_{V_k}^\dagger \\
& + \alpha_5 \hat{a}_{V_{12}}^\dagger \hat{a}_{H_9}^\dagger \hat{a}_{H_k}^\dagger + \alpha_6 \hat{a}_{V_{12}}^\dagger \hat{a}_{H_9}^\dagger \hat{a}_{V_k}^\dagger + \alpha_7 \hat{a}_{V_{12}}^\dagger \hat{a}_{V_9}^\dagger \hat{a}_{V_k}^\dagger + \alpha_8 \hat{a}_{V_{12}}^\dagger \hat{a}_{V_9}^\dagger \hat{a}_{H_k}^\dagger) |\text{vac.}\rangle.
\end{aligned} \tag{42}$$

The three-photon Toffoli gate is completed. (ii) Equation (39) evolves into eight-fold output state

$$\begin{aligned}
|\Xi_{12,10,k}^+\rangle_3 = \frac{1}{64} & (\alpha_1 \hat{a}_{H_{12}}^\dagger \hat{a}_{H_{10}}^\dagger \hat{a}_{H_k}^\dagger + \alpha_2 \hat{a}_{H_{12}}^\dagger \hat{a}_{H_{10}}^\dagger \hat{a}_{V_k}^\dagger + \alpha_3 \hat{a}_{H_{12}}^\dagger \hat{a}_{V_{10}}^\dagger \hat{a}_{H_k}^\dagger + \alpha_4 \hat{a}_{H_{12}}^\dagger \hat{a}_{V_{10}}^\dagger \hat{a}_{V_k}^\dagger \\
& + \alpha_5 \hat{a}_{V_{12}}^\dagger \hat{a}_{H_{10}}^\dagger \hat{a}_{H_k}^\dagger + \alpha_6 \hat{a}_{V_{12}}^\dagger \hat{a}_{H_{10}}^\dagger \hat{a}_{V_k}^\dagger + \alpha_7 \hat{a}_{V_{12}}^\dagger \hat{a}_{V_{10}}^\dagger \hat{a}_{V_k}^\dagger + \alpha_8 \hat{a}_{V_{12}}^\dagger \hat{a}_{V_{10}}^\dagger \hat{a}_{H_k}^\dagger) |\text{vac.}\rangle.
\end{aligned} \tag{43}$$

The three-photon Toffoli gate is also completed. (iii) Equation (40) evolves into eight-fold output state

$$\begin{aligned}
|\Xi_{11,9,k}^-\rangle_3 = \frac{1}{64} & (\alpha_1 \hat{a}_{H_{11}}^\dagger \hat{a}_{H_9}^\dagger \hat{a}_{H_k}^\dagger + \alpha_2 \hat{a}_{H_{11}}^\dagger \hat{a}_{H_9}^\dagger \hat{a}_{V_k}^\dagger - \alpha_3 \hat{a}_{H_{11}}^\dagger \hat{a}_{V_9}^\dagger \hat{a}_{H_k}^\dagger - \alpha_4 \hat{a}_{H_{11}}^\dagger \hat{a}_{V_9}^\dagger \hat{a}_{V_k}^\dagger \\
& + \alpha_5 \hat{a}_{V_{11}}^\dagger \hat{a}_{H_9}^\dagger \hat{a}_{H_k}^\dagger + \alpha_6 \hat{a}_{V_{11}}^\dagger \hat{a}_{H_9}^\dagger \hat{a}_{V_k}^\dagger - \alpha_7 \hat{a}_{V_{11}}^\dagger \hat{a}_{V_9}^\dagger \hat{a}_{H_k}^\dagger - \alpha_8 \hat{a}_{V_{11}}^\dagger \hat{a}_{V_9}^\dagger \hat{a}_{V_k}^\dagger) |\text{vac.}\rangle.
\end{aligned} \tag{44}$$

And then an HWP^{0°} is set in the output mode 9 to complete the three-photon Toffoli gate. (iv) Equation (41) evolves into eight-fold output state

$$\begin{aligned}
|\Xi_{11,10,k}^-\rangle_3 = \frac{1}{64} & (\alpha_1 \hat{a}_{H_{11}}^\dagger \hat{a}_{H_{10}}^\dagger \hat{a}_{H_k}^\dagger + \alpha_2 \hat{a}_{H_{11}}^\dagger \hat{a}_{H_{10}}^\dagger \hat{a}_{V_k}^\dagger - \alpha_3 \hat{a}_{H_{11}}^\dagger \hat{a}_{V_{10}}^\dagger \hat{a}_{H_k}^\dagger - \alpha_4 \hat{a}_{H_{11}}^\dagger \hat{a}_{V_{10}}^\dagger \hat{a}_{V_k}^\dagger \\
& + \alpha_5 \hat{a}_{V_{11}}^\dagger \hat{a}_{H_{10}}^\dagger \hat{a}_{H_k}^\dagger + \alpha_6 \hat{a}_{V_{11}}^\dagger \hat{a}_{H_{10}}^\dagger \hat{a}_{V_k}^\dagger - \alpha_7 \hat{a}_{V_{11}}^\dagger \hat{a}_{V_{10}}^\dagger \hat{a}_{V_k}^\dagger - \alpha_8 \hat{a}_{V_{11}}^\dagger \hat{a}_{V_{10}}^\dagger \hat{a}_{H_k}^\dagger) |\text{vac.}\rangle.
\end{aligned} \tag{45}$$

And then an HWP^{0°} is set in the output mode 10 to complete the three-photon Toffoli gate.

Based on above orthogonal eight-fold states described by Equations (42-45), one can find that our proposal can be achieved in the coincidence basis with a higher success probability ($64 \times 1/64^2 = 1/64$) than the simplified CNOT-based one ($1/72$) [33, 34] and the one without a decomposition-based approach ($1/133$) [73]. In addition, optical single-qudit operation ensembles X_a, X_b, \dots, X_n can be achieved by employing a sequence of PBSs, and the linear optical n -control-photon Toffoli gate can be implemented in principle (see Figure 7).

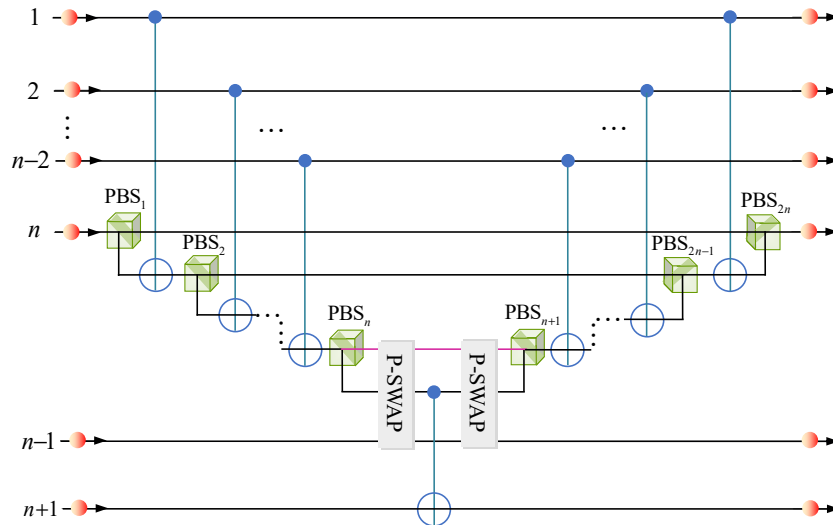


FIG. 7: Implementation of an $(n + 1)$ -photon Toffoli gate.

IV. DISCUSSION AND CONCLUSION

The optimal cost of a Toffoli gate is six CNOT gates using the standard decomposition-based approach in qubit system [62]. The theoretical lower bound of a Toffoli gate is five two-qubit gates in qubit system [63]. Ralph *et al.* [33] first reduced the cost of a Toffoli gate to three qubit-qudit CNOT gates by introducing a qutrit. Using the same idea as the works in Refs. [33, 34], we designed an alternative the quantum circuit to implement the Toffoli gate with a higher success probability based on the P-SWAP gates, which required the same number of qubit-qudit gates as the protocols in Refs. [33, 34]. The required qubit-qudit entangled gates are all nearest neighbors in our construction of the three-qubit Toffoli gate. Note that the nearest-neighbor quantum gate where each qubit interacts only with its nearest neighbors requires less resource overhead than the long-range one. For example, a long-range CNOT gate acting on the first qubit and the third qubit is constructed by four nearest-neighbor CNOT gates [86]. In addition, $(2n - 1)$ qubit-qudit gates and $(2n - 2)$ single-qudit gates can simulate an n -control-qubit Toffoli gate in higher-dimensional spaces.

Linear optics has inherent probability characteristics for the implementation of controlled quantum gates. With the help of an additional entangled photon pair [75, 78] or a single photon [79], optical CNOT gate with a success probability of $1/4$ or $1/8$ can be realistically implemented. Without auxiliary photons, CNOT gate with a success probability of $1/9$ has been experimentally demonstrated in linear optics [81–84]. Remarkably, the success probability of our P-SWAP-based CNOT gate is enhanced to $1/8$ without additional photons. Moreover, the success probability of our P-SWAP-based Toffoli gate ($1/64$) is higher than the CNOT-based protocols ($1/72$) [33, 34] and it is also higher than the no-decomposition-based one ($1/133$) [73].

The multi-level system is essential to realize our schemes. In optical system, we can encode polarization DOF of photons as two computational qubits and spatial-mode DOF as the qudit (extra level). We can also encode these levels on orbital angular momentum of photons. Besides, diamond nitrogen-vacancy defect center [87, 88] and superconducting system [89, 90] can also provide available multiple levels to implement the universal quantum gates due to their long coherence time and flexible manipulation.

In summary, by introducing higher-dimensional spaces, we proposed simplified CNOT and Toffoli gates. A three-qubit Toffoli gate can be simulated with two P-SWAP, one CNOT, and two single-qutrit gates. $(2n - 1)$ qubit-qudit gates and $(2n - 2)$ single-qudit gates are sufficient for constructing an n -control-qubit Toffoli gate. Following the simplified synthesis, as a feasible example, linear optics architectures for implementing CNOT and Toffoli gates were designed with a higher success probability.

ACKNOWLEDGMENTS

This work is supported by the National Natural Science Foundation of China under Grant No. 11604012, the Fundamental Research Funds for the Central Universities under Grants No. FRF-TP-19-011A3 and No. 230201506500024, and a grant from the China Scholarship Council. L.-C.K. is supported by the Ministry of Education and the National Research Foundation Singapore.

-
- [1] A. Barenco, C. H. Bennett, R. Cleve, D. P. DiVincenzo, N. Margolus, P. Shor, T. Sleator, J. A. Smolin, H. Weinfurter, *Phys. Rev. A* **1995**, *52*, 3457.
 - [2] L. K. Grover, *Phys. Rev. Lett.* **1997**, *79*, 325.
 - [3] P. W. Shor, *SIAM Rev.* **1999**, *41*, 303.
 - [4] G. L. Long, *Phys. Rev. A* **2001**, *64*, 022307.
 - [5] C. Figgatt, D. Maslov, K. Landsman, N. M. Linke, S. Debnath, C. Monroe, *Nat. Commun.* **2017**, *8*, 1918.
 - [6] Y. Nam, Y. Su, D. Maslov, *npj Quantum Inform.* **2020**, *6*, 26.
 - [7] J. W. Pan, Z. B. Chen, C. Y. Lu, H. Weinfurter, A. Zeilinger, M. Żukowski, *Rev. Mod. Phys.* **2012**, *84*, 777.
 - [8] P. H. Niu, Z. R. Zhou, Z. S. Lin, Y. B. Sheng, L. G. Yin, G. L. Long, *Sci. Bull.* **2018**, *63*, 1345–1350.
 - [9] S. S. Chen, L. Zhou, W. Zhong, Y. B. Sheng, *Sci. China-Phys. Mech. Astron.* **2018**, *61*, 90312.
 - [10] Z. X. Cui, W. Zhong, L. Zhou, Y. B. Sheng, *Sci. China-Phys. Mech. Astron.* **2019**, *62*, 110311.
 - [11] R. Qi, Z. Sun, Z. Lin, P. Niu, W. Hao, L. Song, Q. Huang, J. Gao, L. Yin, G. L. Long, *Light Sci. Appl.* **2019**, *8*, 22.
 - [12] Z. Gao, T. Li, Z. Li, *Sci. China-Phys. Mech. Astron.* **2020**, *63*, 120311.
 - [13] L. Zhou, Y. B. Sheng, G. L. Long, *Sci. Bull.* **2020**, *65*, 12–20.
 - [14] T. Li, G. L. Long, *New J. Phys.* **2020**, *22*, 063017.
 - [15] Z. R. Zhou, Y. B. Sheng, P. H. Niu, L. G. Yin, G. L. Long, L. Hanzo, *Sci. China-Phys. Mech. Astron.* **2020**, *63*, 230362.
 - [16] Y. F. Yan, L. Zhou, W. Zhong, Y. B. Sheng, *Front. Phys.* **2021**, *16*, 11501.

- [17] N. Gisin, G. Ribordy, W. Tittel, H. Zbinden, *Rev. Mod. Phys.* **2002**, *74*, 145.
- [18] M. A. Nielsen, I. L. Chuang, *Quantum Computation and Quantum Information: 10th Anniversary Edition*, (Cambridge University Press, Cambridge, England, 2010).
- [19] V. V. Shende, I. L. Markov, S. S. Bullock, *Phys. Rev. A* **2004**, *69*, 062321.
- [20] M. Reck, A. Zeilinger, H. J. Bernstein, P. Bertani, *Phys. Rev. Lett.* **1994**, *73*, 58.
- [21] N. Khaneja, S. J. Glaser, *J. Chem. Phys.* **2001**, *267*, 11–23.
- [22] M. Möttönen, J. J. Vartiainen, V. Bergholm, M. M. Salomaa, *Phys. Rev. Lett.* **2004**, *93*, 130502.
- [23] S. S. Bullock, G. K. Brennen, *J. Math. Phys.* **2004**, *45*, 2447.
- [24] V. V. Shende, S. S. Bullock, I. L. Markov, *IEEE Trans. Comput. Aided Des. Integr. Circuits Syst.* **2006**, *25*, 1000–1010.
- [25] D. D'Alessandro, F. Albertini, *J. Phys. A-Math. Theor.* **2007**, *40*, 2439.
- [26] Y. M. Di, H. R. Wei, *Phys. Rev. A* **2013**, *87*, 012325.
- [27] R. Iten, R. Colbeck, I. Kukuljan, J. Home, M. Christandl, *Phys. Rev. A* **2016**, *93*, 032318.
- [28] A. Sawicki, *Quantum Inf. Comput.* **2016**, *16*, 291–312.
- [29] W. R. Clements, P. C. Humphreys, B. J. Metcalf, W. S. Kolthammer, I. A. Walmsley, *Optica* **2016**, *3*, 1460–1465.
- [30] F. Vatan, C. Williams, *Phys. Rev. A* **2004**, *69*, 032315.
- [31] G. Vidal, C. M. Dawson, *Phys. Rev. A* **2004**, *69*, 010301(R).
- [32] V. V. Shende, S. S. Bullock, I. L. Markov, *Phys. Rev. A* **2004**, *70*, 012310.
- [33] T. C. Ralph, K. J. Resch, A. Gilchrist, *Phys. Rev. A* **2007**, *75*, 022313.
- [34] B. P. Lanyon, M. Barbieri, M. P. Almeida, T. Jennewein, T. C. Ralph, K. J. Resch, G. J. Pryde, J. L. O'Brien, A. Gilchrist, A. G. White, *Nat. Phys.* **2009**, *5*, 134.
- [35] A. Fedorov, L. Steffen, M. Baur, M. P. da Silva, A. Wallraff, *Nature* **2012**, *481*, 170.
- [36] K. Liu, W. D. Li, W. Z. Zhang, P. Shi, C. N. Ren, Y. J. Gu, *Acta Phys. Sin-Ch Ed* **2012**, *61*, 120301.
- [37] W. D. Li, Y. J. Gu, K. Liu, Y. H. Lee, Y. Z. Zhang, *Phys. Rev. A* **2013**, *88*, 034303.
- [38] W. Q. Liu, H. R. Wei, *New J. Phys.* **2020**, *22*, 063026.
- [39] W. Q. Liu, H. R. Wei, L. C. Kwek, *Phys. Rev. Appl.* **2020**, *14*, 054057.
- [40] A. Sawicki, K. Karnas, *Phys. Rev. A* **2017**, *95*, 062303.
- [41] A. Sawicki, K. Karnas, *Ann. Henri. Poincaré* **2017**, *18*, 3515.
- [42] K. Lemr, K. Bartkiewicz, A. Černoch, M. Dušek, J. Soubusta, *Phys. Rev. Lett.* **2015**, *114*, 153602.
- [43] A. Babazadeh, M. Erhard, F. Wang, M. Malik, R. Nouroozi, M. Krenn, A. Zeilinger, *Phys. Rev. Lett.* **2017**, *119*, 180510.
- [44] X. Gao, M. Erhard, A. Zeilinger, M. Krenn, *Phys. Rev. Lett.* **2020**, *125*, 050501.
- [45] Y. Wang, Z. Hu, B. C. Sanders, S. Kais, *Front. Phys. (Lausanne)* **2020**, *8*, 479.
- [46] N. J. Cerf, M. Bourennane, A. Karlsson, N. Gisin, *Phys. Rev. Lett.* **2002**, *88*, 127902.
- [47] B. P. Lanyon, T. J. Weinhold, N. K. Langford, J. L. O'Brien, K. J. Resch, A. Gilchrist, A. G. White, *Phys. Rev. Lett.* **2008**, *100*, 060504.
- [48] M. Malik, M. Erhard, M. Huber, M. Krenn, R. Fickler, A. Zeilinger, *Nat. Photonics* **2016**, *10*, 248.
- [49] Y. Zhang, M. Agnew, T. Roger, F. S. Roux, T. Konrad, D. Faccio, J. Leach, A. Forbes, *Nat. Commun.* **2017**, *8*, 632.
- [50] F. Wang, M. Erhard, A. Babazadeh, M. Malik, M. Krenn, A. Zeilinger, *Optica* **2017**, *4*, 1462.
- [51] X. M. Hu, Y. Guo, B. H. Liu, Y. F. Huang, C. F. Li, G. C. Guo, *Sci. Adv.* **2018**, *4*, eaat9304.
- [52] Y. H. Luo, H. S. Zhong, M. Erhard, X. L. Wang, L. C. Peng, M. Krenn, X. Jiang, L. Li, N. L. Liu, C. Y. Lu, A. Zeilinger, J. W. Pan, *Phys. Rev. Lett.* **2019**, *123*, 070505.
- [53] X. M. Hu, C. Zhang, B. H. Liu, Y. Cai, X. J. Ye, Y. Guo, W. B. Xing, C. X. Huang, Y. F. Huang, C. F. Li, G. C. Guo, *Phys. Rev. Lett.* **2020**, *125*, 230501.
- [54] V. D'ambrosio, N. Spagnolo, L. D. Re, S. Slussarenko, Y. Li, L. C. Kwek, L. Marrucci, S. P. Walborn, L. Aolita, F. Sciarrino, *Nat. Commun.* **2013**, *4*, 2432.
- [55] Y. Shi, *Quantum Inf. Comput.* **2002**, *3*, 84.
- [56] L. Mattioli, A. Sawicki, **2021**, arXiv:2110.04210.
- [57] A. Sawicki, L. Mattioli, Z. Zimborás, **2021**, arXiv:2111.03862.
- [58] D. G. Cory, M. Price, W. Maas, E. Knill, R. Laflamme, W. H. Zurek, T. F. Havel, S. S. Somaroo, *Phys. Rev. Lett.* **1998**, *81*, 2152.
- [59] M. D. Reed, L. DiCarlo, S. E. Nigg, L. Sun, L. Frunzio, S. M. Girvin, R. J. Schoelkopf, *Nature* **2012**, *482*, 382.
- [60] A. Paetznick, B. W. Reichardt, *Phys. Rev. Lett.* **2013**, *111*, 090505.
- [61] J. Guillaud, M. Mirrahimi, *Phys. Rev. X* **2019**, *9*, 041053.
- [62] V. V. Shende, I. L. Markov, *Quantum Inf. Comput.* **2008**, *9*, 461.
- [63] N. Yu, R. Duan, M. Ying, *Phys. Rev. A* **2013**, *88*, 010304(R).
- [64] N. Yu, M. Ying, *Phys. Rev. A* **2015**, *91*, 032302.
- [65] E. O. Kiktenko, A. S. Nikolaeva, P. Xu, G. V. Shlyapnikov, A. K. Fedorov, *Phys. Rev. A* **2020**, *101*, 022304.
- [66] M. Mičuda, M. Sedlak, I. Straka, M. Miková, M. Dušek, M. Ježek, J. Fiurášek, *Phys. Rev. Lett.* **2013**, *111*, 160407.
- [67] M. Mičuda, M. Miková, I. Straka, M. Sedlák, M. Dušek, M. Ježek, J. Fiurášek, *Phys. Rev. A* **2015**, *92*, 032312.
- [68] S. Ru, Y. Wang, M. An, F. Wang, P. Zhang, F. Li, *Phys. Rev. A* **2021**, *103*, 022606.
- [69] T. Monz, K. Kim, W. Hänsel, M. Riebe, A. Villar, P. Schindler, M. Chwalla, M. Hennrich, R. Blatt, *Phys. Rev. Lett.* **2009**, *102*, 040501.
- [70] I. I. Beterov, I. N. Ashkarin, E. A. Yakshina, D. B. Tretyakov, V. M. Entin, I. I. Ryabtsev, P. Cheinet, P. Pillet, M. Saffman, *Phys. Rev. A* **2018**, *98*, 042704.
- [71] H. Levine, A. Keesling, G. Semeghini, A. Omran, T. T. Wang, S. Ebadi, H. Bernien, M. Greiner, V. Vuletić, H. Pichler, M. D. Lukin, *Phys. Rev. Lett.* **2019**, *123*, 170503.

- [72] M. J. Gullans, J. R. Petta, *Phys. Rev. B* **2019**, *100*, 085419.
- [73] J. Fiurášek, *Phys. Rev. A* **2006**, *73*, 062313.
- [74] T. B. Pittman, B. C. Jacobs, J. D. Franson, *Phys. Rev. A* **2001**, *64*, 062311.
- [75] X. H. Bao, T. Y. Chen, Q. Zhang, J. Yang, H. Zhang, T. Yang, J. W. Pan, *Phys. Rev. Lett.* **2007**, *98*, 170502.
- [76] J. P. Li, X. Gu, J. Qin, D. Wu, X. You, H. Wang, C. Schneider, S. Höfling, Y. H. Huo, C. Y. Lu, N. L. Liu, L. Li, J. W. Pan, *Phys. Rev. Lett.* **2021**, *126*, 140501.
- [77] W. B. Gao, A. M. Goebel, C. Y. Lu, H. N. Dai, C. Wagenknecht, Q. Zhang, B. Zhao, C. Z. Peng, Z. B. Chen, Y. A. Chen, J. W. Pan, *Proc. Natl. Acad. Sci. USA* **2010**, *107*, 20869.
- [78] S. Gasparoni, J. W. Pan, P. Walther, T. Rudolph, A. Zeilinger, *Phys. Rev. Lett.* **2004**, *93*, 020504.
- [79] J. Zeuner, A. N. Sharma, M. Tillmann, R. Heilmann, M. Gräfe, A. Moqanaki, A. Szameit, P. Walther, *npj Quantum Inform.* **2018**, *4*, 13.
- [80] T. C. Ralph, N. K. Langford, T. B. Bell, A. G. White, *Phys. Rev. A* **2002**, *65*, 062324.
- [81] J. L. O'Brien, G. J. Pryde, A. G. White, T. C. Ralph, D. Branning, *Nature* **2003**, *426*, 264–267.
- [82] N. K. Langford, T. J. Weinhold, R. Prevedel, K. J. Resch, A. Gilchrist, J. L. O'Brien, G. J. Pryde, A. G. White, *Phys. Rev. Lett.* **2005**, *95*, 210504.
- [83] N. Kiesel, C. Schmid, U. Weber, R. Ursin, H. Weinfurter, *Phys. Rev. Lett.* **2005**, *95*, 210505.
- [84] R. Okamoto, H. F. Hofmann, S. Takeuchi, K. Sasaki, *Phys. Rev. Lett.* **2005**, *95*, 210506.
- [85] X. Q. Zhou, T. C. Ralph, P. Kalasuwan, M. Zhang, A. Peruzzo, B. P. Lanyon, J. L. O'Brien, *Nat. Commun.* **2011**, *2*, 413.
- [86] G. F. Viamontes, I. L. Markov, J. P. Hayes, *Quantum circuit simulation*, (Springer Science, New York, 2009).
- [87] Z. L. Xiang, S. Ashhab, J. Q. You, F. Nori, *Rev. Mod. Phys.* **2013**, *85*, 623.
- [88] G. Waldherr, Y. Wang, S. Zaiser, M. Jamali, T. Schulte-Herbrüggen, H. Abe, T. Ohshima, J. Isoya, J. F. Du, P. Neumann, J. Wrachtrup, *Nature* **2014**, *506*, 204.
- [89] M. J. Peterer, S. J. Bader, X. Jin, F. Yan, A. Kamal, T. J. Gudmundsen, P. J. Leek, T. P. Orlando, W. D. Oliver, S. Gustavsson, *Phys. Rev. Lett.* **2015**, *114*, 010501.
- [90] T. Bækkegaard, L. B. Kristensen, N. J. S. Loft, C. K. Andersen, D. Petrosyan, N. T. Zinner, *Sci. Rep.* **2019**, *9*, 13389.